Temperature Dependent Imaging of Solar Cell Losses

Rebekka Eberle[1, a)], Wolfram Kwapil[1,2,b)] and Martin C. Schubert[1]

[1]*Fraunhofer Institute for Solar Energy Systems ISE, Heidenhofstraße 2, 79110 Freiburg, Germany*
[2]*Freiburger Materialforschungszentrum (FMF), Albert-Ludwigs-Universität Freiburg, Stefan-Meier-Straße 21, 79104 Freiburg, Germany*

[a)]Corresponding author: rebekka.eberle@ise.fraunhofer.de
[b)]wolfram.kwapil@ise.fraunhofer.de

Abstract. GLOBAL cell efficiencies are measured at standardized testing conditions (STC) to be able to compare technology improvements worldwide in a systematic manner. However, these STC are rarely met in real operation conditions of solar cells as especially temperature and irradiation intensity differ a lot to laboratory standards. In this study we present an approach to characterize the temperature-dependent behavior of solar cells with spatial resolution. Therefore, techniques for imaging of series resistance, short-circuit current and a Local IV analysis are performed at different temperatures. At each of these a cell analysis is conducted to evaluate the cell's efficiency and its losses as well as to calculate temperature coefficients of cell parameters. Especially due the spatial resolution, information about the influence of different cell areas on the cell's performance at varying temperatures can be gained as a valuable basis for further cell improvements. Good agreement of temperature coefficients calculated from global measurements and averaged from maps of fitted values assuming a linear behavior with temperature show the applicability of our approach which enables efficiency optimizations of silicon solar cells for non-ideal operation conditions.

INTRODUCTION

Usually, the efficiency of silicon solar cells is characterized in test laboratories at standard testing conditions (STC) of 25°C with an irradiation intensity of 1000 W/m^2 and a standard spectrum to simulate an illumination equivalent to 1 sun at AM 1.5g [1,2]. These conditions are also used to predict the efficiency of a solar cell and its losses due to non-ideal optical, series resistance R_S, shunt or *open circuit voltage* V_{OC} properties [3]. In this contribution we combine the measurement approaches of CDCR [4], Local IV [5] and SR-LBIC [6] to gather spatially resolved results of solar cell parameters to calculate the efficiency and losses of a solar cell for further optimization.

Usual studies dealing with cell performance do not consider varying temperatures though these influence the output of a solar cell significantly. A change in temperature causes an alteration of a cell's operating characteristics as the temperature influences the energy level of the band gap E_g [7]. Therefore increased temperature results in a rise of *short-circuit current density* j_{SC} and a severe decrease of V_{OC} as recombination in general increases, leading to reduced cell efficiencies [8-14]. Eventually these effects also have an impact on module output as solar cells are usually optimized for STC. However, STC rarely exist in real operation, predicted energy outputs of modules can hardly be reached.

For this study we improved the above mentioned measurement techniques to analyze temperature dependent solar cell efficiencies as well as losses on whole cells with high spatial resolution. By an analysis of maps of multicrystalline silicon samples and their temperature dependent parameters optimization of cells for real operation conditions will be made possible.

SiliconPV 2018, The 8th International Conference on Crystalline Silicon Photovoltaics
AIP Conf. Proc. 1999, 020005-1–020005-6; https://doi.org/10.1063/1.5049244
Published by AIP Publishing. 978-0-7354-1715-1/$30.00

MATERIAL AND METHODS

For the analysis of solar cell losses, which we call *Total Cell Analysis (TCA),* three approaches are combined [3]: Via the method of *coupled determination of dark saturation current* and *series resistance (CDCR)* which uses photoluminescence (PL) imaging, the (*dark) saturation current density* j_0 as well as the *series resistance* R_S can be mapped [4]. Local IV analysis via dark lock-in thermography (DLIT) is used to calculate the *saturation current due to diffusion current density* j_{01} and due to *recombination current density* j_{02} as well as *diode ideality factor* n_2, the *pseudo fill factor PFF* and power losses due to shunts G_{shunt} [5]. At last, imaging of *short circuit current density* j_{SC} via spectrally resolved light beam-induced current (SR-LBIC) measurements is conducted to determine the spatially resolved j_{SC} and optical losses [6]. Each of these methods delivers results in high spatial resolution which is needed to analyze the local influence of various wafer and cell areas on the cell's performance. Further details of the computation of parameter maps can be found in the mentioned literature. With the aforementioned results the local cell efficiency is calculated according to Equation (1):

$$\eta_{xy} = j_{SC,xy} \cdot V_{OC,xy} \cdot FF_{xy} \tag{1}$$

Here FF_{xy} is calculated for each pixel by a consideration of series resistance losses to local PFF_{xy} which is gathered via DLIT. For $V_{OC,xy}$ two measurement techniques can be applied: Firstly, it can be calculated with local values of j_0 from CDCR [4]. This method yields a high spatial resolution, but leads to reduced contrast due to lateral balancing currents and therefore to rather qualitative results for local analysis. Secondly, also DLIT yields maps of $V_{OC,xy}$ with correct values which have the drawback of a lower quality due to optical blurring [5]. Due to the spatial resolution an optimal value for each parameter can be gained by a comparison with best cell areas. This kind of loss analysis is done for many different parameters like R_S, j_{SC}, PFF, FF_0 or V_{OC} to calculate an optimum *efficiency* $\eta_{optimum}$ with the power density of incident photons P_γ and to analyse several loss channels which contribute to the difference between actual and optimal efficiency:

$$\eta_{optimum} = \frac{PJ_{SC,max} \cdot V_{OC,max} \cdot FF_{0,max}}{P_\gamma} = Pj_{SC,max} \cdot V_{OC,max} \cdot FF_{0,max} \tag{2}$$

For this study the approach by Michl et al. [3] was developed further to be able to characterize solar cells for realistic operation conditions. The measurement setups were improved by a change in the temperature adjustment of the used measurement chucks. Built-in Peltier cooling systems regulate the cell's temperature with an uncertainty of ±0.4 Kelvin for a temperature range of 15 to 75°C during characterization. The setups as well as all evaluation algorithms were adapted for determination of cell parameters and losses to consider the actual temperature of measured solar cells.

The loss analysis of this study was carried out on p-type multicrystalline (mc) Passivated Emitter and Rear cells (PERC) with a base resistivity of ~1.8 Ωcm. The measurements were conducted at temperatures of 15°C to maximum 75°C (no degradation was observed for the analyzed samples) and a spatially resolved analysis of the solar cell performances, losses and their temperature behavior was accomplished. Therefore, the data of temperature dependent cell parameters was fitted assuming a linear behavior with temperature [14].

RESULTS

A high number of various parameter maps are resulting from TCA describing the performance of a solar cell. To illustrate some basic characteristics of the studied solar cells three different maps gathered by TCA at 25°C of a multicrystalline sample are shown in Fig. 1. To see the structure of the base material Fig. 1 a) depicts a map of the *minority carrier lifetime* τ indicating several dislocation clusters and grains with low initial lifetime values. The metallization is checked in Fig. 1 b), you can see the spatially resolved *series resistance* R_S gathered by CDCR which shows increased R_S due to very thin fingers and lost contact between metal and cell surface in the lower part of the image. Figure 1 c) illustrates the most important result of TCA analysis by showing the efficiency map which is calculated with maps of j_{SC}, V_{OC} and FF according to *Eq. (1)*. Small patterns with decreased efficiency are obvious which correlate with areas of low initial lifetime seen in the lifetime map of Fig. 1 a).

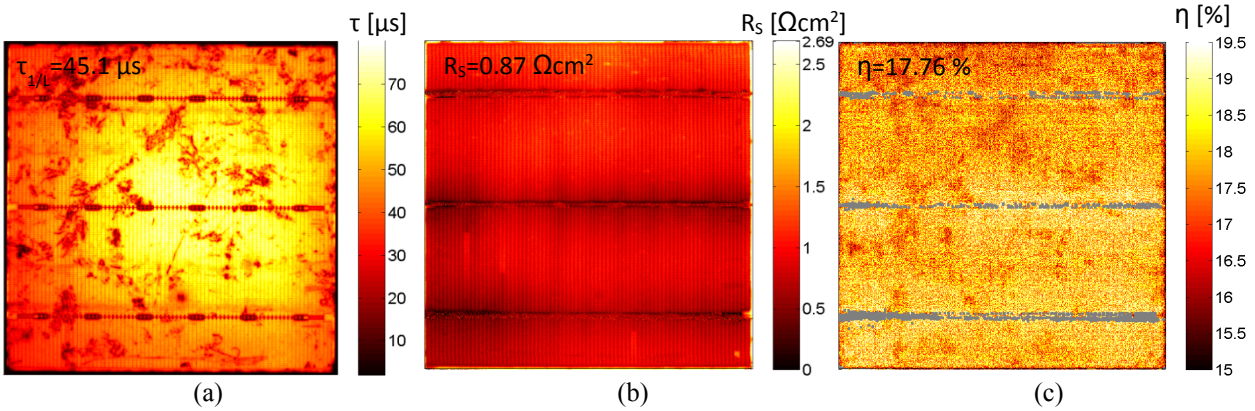

FIGURE 1. a) Lifetime map of mc-Si PERC sample, b) map of series resistance R_S at 25°C as well as c) of the efficiency η.

To analyze the consistency of the TCA itself measurements at STC are compared with results gathered by global analyses of the same sample shown in **Table 1**. For the local measurement approaches parameters are averaged arithmetically (respectively harmonically for V_{OC}) over the whole image [3].

TABLE 1. Comparison of cell parameters gathered by global measurement techniques and by averaging of local analysis methods at STC of 25°C and irradiation intensity of ~1sun.

Parameters gathered via	V_{oc} (mV)	j_{sc} (mA/cm²)	FF (%abs)	R_S (Ωcm²)	η (%abs)
Global cell characterization	639.9	36.4	76.5	0.93	17.82
Image average	643.1	36.2	76.5	0.87	17.76

TCA was not only conducted at STC, but also at temperatures from 15°C up to 75°C. Using these measurements and assuming linear temperature behavior for a limited temperature range according to [7], temperature coefficients of j_{SC}, V_{OC}, *efficiency* as well as *FF* are calculated using a linear fit of all pixels [14]. Figure 2 shows maps of several temperature coefficients: a) depicts $TC(j_{SC})$; a comparison with Fig. 1 a) leads to the conclusion that low lifetime areas have an increased temperature sensibility, j_{SC} rises exceptionally strong for these grains as these areas are not limited by Auger recombination. In contrast to $TC(j_{SC})$ Fig. 2 b) depicts that $TC(V_{OC})$ decreases for these same areas in absolute values which might be caused an overall lower level of V_{OC} which limits the change with temperature. The most important result of the analysis is shown in Fig. 2 c) which shows the spatially resolved temperature-dependent behavior of η. Here the same behavior as for $TC(V_{OC})$ is observed as also the temperature sensibility of efficiency decreases in areas with low initial lifetime.

The consistency of our approach is shown by reasonable agreement between temperature coefficients which were calculated with globally gathered cell parameters and values which are averaged arithmetically from calculated spatially resolved analysis (for V_{OC}, values are averaged harmonically), these results can be seen in Table 2 for V_{OC}, j_{SC}, FF, R_S and η.

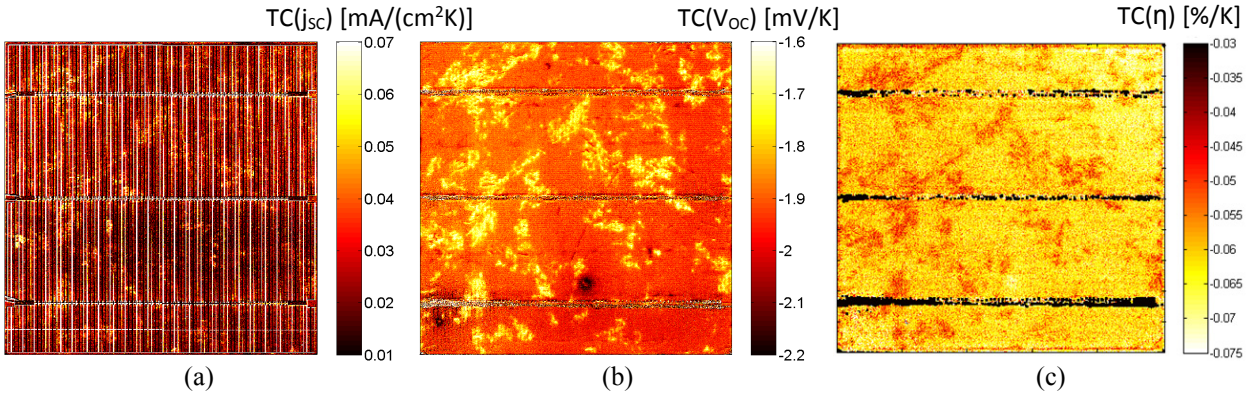

FIGURE 2. a) Map of temperature coefficient of *short-circuit current density TC(j_{SC}),* b) of *open-circuit voltage TC(V_{OC})* calculated from CDCR measurements for qualitative analysis as well as c) of *efficiency TC(η).*

TABLE 2. Comparison of temperature coefficients of different cell parameters from IV curves and values fitted linearly from calculated parameter maps.

Temperature coefficient of	V_{oc} (mV/K)		j_{sc} (mA/cm²K)	FF (%$_{abs}$/K)	R_S (mΩcm²/K)	η (%$_{abs}$/K)
Global cell characterization	-1.92		0.025	-0.09	5.4	-0.08
Image average	CDCR -1.90	DLIT -1.87	0.028	-0.08	5.5	-0.06

For a further evaluation of the spatially resolved maps of TCA Fig. 3 depicts the histograms of V_{OC} (a)) as well as η (b)) for the measured temperatures from 15°C to 75°C including medians at each measurement point; both parameters are chosen due to their significant importance for evaluation of cell performances. For V_{OC} one can see a very similar distribution of values for temperatures from 15°C to 50°C as the shape of the histogram is always quite similar as well as a linear change of the median which indicates a stable linear temperature behavior of most pixels. An exception is the behavior at 75°C as especially the V_{OC}-distribution is significantly sharper than for the other temperatures, the width of the histogram is decreased. The observed behavior might be caused by *Shockley-Read-Hall (SRH)* recombination [15, 16] which limits the change in V_{OC} to a distinct level. A very different behavior can be seen for values of η for all pixels: the histogram shape at 15°C and 25°C look quite similar with one local peak and a very broad distribution of η. However, for 50°C and 75°C this distribution alters as the width of the histogram significantly decreases indicating a non-perfect linear behavior for a significant number of pixels. This distribution is influenced by the temperature-dependent behavior of V_{OC}, as seen in Fig. 3 a); V_{OC} shows the highest relative change with temperature compared to j_{SC} and FF and is therefore the most prominent factor having an impact on the final efficiency and its temperature-dependent behavior.

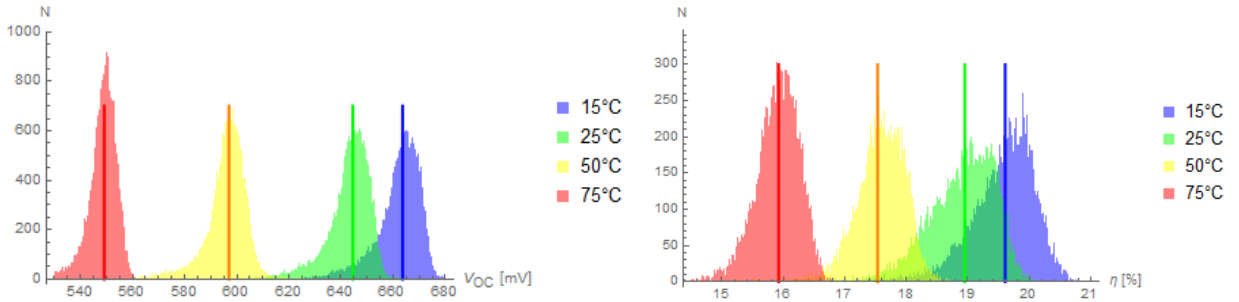

FIGURE 3. a) Histogram of the distribution of V_{OC} for all pixels at four measured temperatures as well as each median, b) median plus histogram of the distribution of η for all pixels from 15°C to 75°C.

TCA delivers not only the actual, but also optimal cell efficiency by a consideration of best cell areas for parameters like j_{SC}, V_{OC}, R_S, *recombination current density* j_0, *FF* and others. Assuming these best values to be valid for the whole sample, an optimal efficiency is calculated which can be compared to the actual one and is shown in Fig. 4 a) for the analyzed solar cell. As expected, actual and measured parameters reduce with temperature, however, the absolute difference between the two efficiencies decreases for increasing temperatures. To explain this behavior Fig. 4 b) illustrates the different loss types at all measured temperatures which contribute to the gap between actual and optimal efficiency. The optical losses are the most critical ones as they lead to a loss in efficiency of up to 2 $\%_{abs}$, however, they decrease with temperature due to a strong rise in j_{SC} compared to pseudo short-circuit current density Pj_{SC} which might be limited by Auger recombination. The losses due to shunts as well as due to R_S show an increase with temperature as especially areas with high R_S show an even stronger rise which is expected from literature [13]. For all other parameters the contribution to efficiency losses seems to decline leading to an overall decreasing loss with temperature. Especially R_S and optical losses have a significant impact due to their high initial loss values and strong direct influence on measured efficiencies. Some minor deviations origin in the evaluation procedure as always the maximum value of the best pixel is assumed to be valid for the whole cell at this temperature.

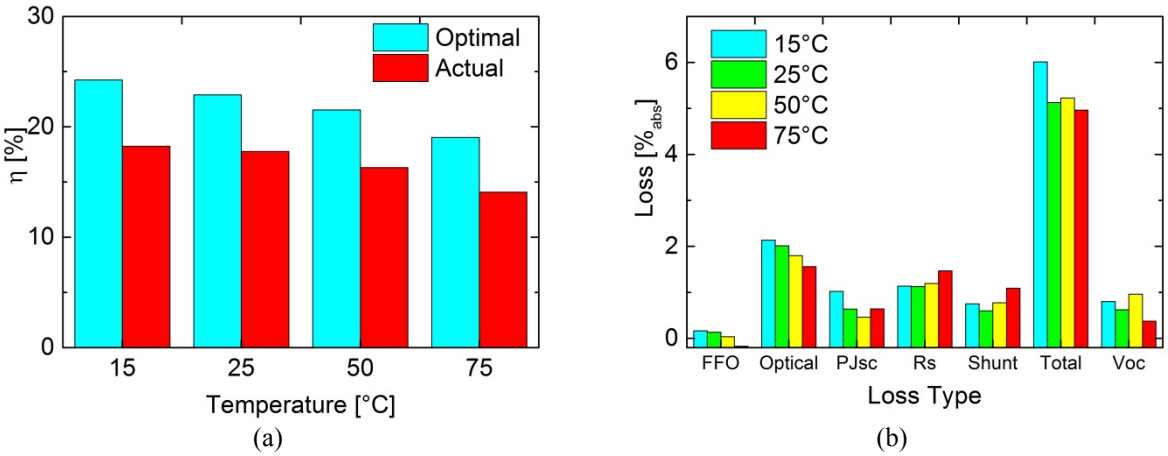

FIGURE 4. a) Chart of optimal efficiency gained from calculations of best areas versus actual efficiency measured at different temperatures, b) Contributions of different loss types to difference between optimal and actual cell efficiency at measured temperatures.

CONCLUSION

The temperature dependent loss analysis is applicable to all kind of solar cells and shows already good agreement with standard solar cell characterization methods in an early step of development. By the spatially resolved analysis at different operating temperatures it is possible to evaluate loss mechanisms contributing to reduced cell efficiencies at real operation conditions. Not only can the behavior of the overall efficiency, but also of different solar cell parameters like j_0, j_{SC} or V_{OC} be studied in a spatial manner. Especially R_S and the optical losses have a significant impact on the reduced efficiency of the final solar cell. The efficiency has a negative temperature coefficient due to a dominating decrease in V_{OC} and increase in R_S and its losses and most losses seem to decline with temperature as the difference between best and other cell areas decreases.

The proposed approach makes it possible to gain knowledge about the spatially resolved temperature-dependent behavior of solar cells. Via maps of local parameters the performance of solar cells at conditions differing from STC temperatures can be studied. This method can be applied to various solar cell concepts with different silicon material to understand their temperature-dependent performance, evaluate the impact of various concepts on local temperature sensibility and to optimize these cells for realistic climatic conditions existing in their destined location of operation.

ACKNOWLEDGMENTS

The authors would like to thank Felix Martin for conducting the LBIC measurements. They acknowledge the financial support by the German Federal Ministry for Economic Affairs and Energy and by industry partners within the project "PROGNOSIS" (contract no. 0324160). Rebekka Eberle appreciates the financial support of the Studienstiftung des deutschen Volkes.

REFERENCES

1. International Electrotechnical Commission, International Standard **2**, IEC 60904-3 (2008).
2. IEC, Photovoltaic devices – part 4: standard reference climatic profiles: spectral responsitivity, incidence angle and module operating temperature measurements. (2011).
3. B. Michl, M. Padilla, I. Geisemeyer, S.T. Haag, F. Schindler, M.C. Schubert and W. Warta, IEEE Journal of Photovoltaics **4**, 1502-1510 (2014).
4. M. Glatthaar, J. Haunschild, M. Kasemann, J. Giesecke, W. Warta and S. Rein, Phys. Status Solidi RRL **4**, 13-15 (2010).
5. O. Breitenstein, Sol. Energy Mater. Sol. Cells **95**, 2933-2936-389 (2011).
6. M. Padilla, B. Michl, B. Thaidigsmann, W. Warta and M.C. Schubert, Sol. Energy Mater. Sol. Cells **120**, 282-288 (2014).
7. M.A. Green, Electronic Letters **18**, 97-98 (1982).
8. J.C.C. Fan, Solar Cells **17**, 309-15 (1986).
9. C. Berthod, R. Strandberg, G.H. Yordanov, H.G. Beyer and J.O. Odden, Energy Procedia **92**, 2-9 (2016)
10. O. Dupre, R. Vaillon, M.A. Green, Solar Energy Materials and Solar Cells **140**, 92-100 (2015).
11. O. Dupre, R. Vaillon, M.A. Green, Solar Energy **140**, 73-82 (2016).
12. P. Löper, D. Pysch, A. Richter, M. Hermle, S. Janz, M. Zacharias and S.W. Glunz, Energy Procedia **27**, 135-42 (2012).
13. M. A. Green, Progress in Photovoltaics: research and Applications **11**, 333-40 (2003).
14. P. Singh and N.M. Ravindra, Solar Energy Materials and Solar Cells **101**, 36-45 (2012).
15. B. Michl, M. Rüdiger, J.A. Giesecke, M. Hermle, W. Warta and M.C. Schubert, Solar Energy Materials and Solar Cells **98**, 441-447 (2012).
16. P. Singh, S.N. Singh, M. Lal and M. Husain, Solar Energy Materials and Solar Cells **92**, 1611-1616 (2008).
17. R. Eberle, S.T. Haag, I. Geisemeyer, M. Padilla and M.C. Schubert, submitted to Journal of Photovoltaics
18. R.N. Hall, Physical Review **87**, 387 (1952).
19. W. Shockley and W. Read, Physical Review **87**, 835 (1952).